

CARBON SYNTHESIS IN STEADY-STATE HYDROGEN AND HELIUM BURNING ON ACCRETING NEUTRON STARS

JEREMY STEVENS^{1,2,3} EDWARD F. BROWN^{1,2,3}, ANDREW CUMMING⁴, RICHARD CYBURT^{1,2,3}, HENDRIK SCHATZ^{1,2,3}

¹ National Superconducting Cyclotron Laboratory, Michigan State University, East Lansing, MI 48824, USA

² The Joint Institute for Nuclear Astrophysics, Michigan State University, East Lansing, MI 48824, USA

³ Dept. of Physics and Astronomy, Michigan State University, East Lansing, MI 48824, USA and

⁴ Dept. of Physics, McGill University, Montreal, QC H3A 2T8, Canada

Draft version May 15, 2014

ABSTRACT

Superbursts from accreting neutron stars probe nuclear reactions at extreme densities ($\rho \approx 10^9 \text{ g cm}^{-3}$) and temperatures ($T > 10^9 \text{ K}$). These bursts (~ 1000 times more energetic than type I X-ray bursts) are most likely triggered by unstable ignition of carbon in a sea of heavy nuclei made during the rp-process of regular type I X-ray bursts (where the accumulated hydrogen and helium are burned). An open question is the origin of sufficient amounts of carbon, which is largely destroyed during the rp-process in X-ray bursts. We explore carbon production in steady-state burning via the rp-process, which might occur together with unstable burning in systems showing superbursts. We find that for a wide range of accretion rates and accreted helium mass fractions large amounts of carbon are produced, even for systems that accrete solar composition. This makes stable hydrogen and helium burning a viable source of carbon to trigger superbursts. We also investigate the sensitivity of the results to nuclear reactions. We find that the $^{14}\text{O}(\alpha, p)^{17}\text{F}$ reaction rate introduces by far the largest uncertainties in the ^{12}C yield.

Subject headings: accretion, accretion disks – nuclear reactions, nucleosynthesis, abundances – stars: neutron – X-Rays: bursts

1. INTRODUCTION

Type I X-ray bursts are thermonuclear flashes of accumulated hydrogen and helium on the surface of an accreting neutron star (Woosley & Taam 1976; Maraschi & Cavaliere 1977; Joss 1977). Nearly a hundred Low Mass X-Ray Binaries (LMXBs) in the Galaxy have shown these events (Galloway et al. 2010), see also the reviews by Lewin et al. (1993, 1997); Bildsten (1998); Schatz & Rehm (2006); Parikh et al. (2013).

A rare class of type I bursts, now called superbursts, were discovered during long term monitoring of LMXBs with the BeppoSAX Wide Field Cameras (Cornelisse et al. 2000, 2002; Kuulkers et al. 2002). These superbursts occur in sources that otherwise exhibit normal type I bursts. Superbursts last about a factor of 1000 longer than regular bursts (a day compared to 10–100 s) and have a factor of 1000 more energy output, typically 10^{42} erg. So far about 22 bursts from 13 sources have been observed (see Keek & in’t Zand (2008); Keek & Heger (2011); Keek et al. (2012)). Recurrence times around a year are estimated but uncertain because of limited observational data (Keek et al. 2006).

Superbursts are thought to be driven by thermonuclear ignition of a deep carbon layer in the liquid ocean of the neutron star (Cumming & Bildsten 2001; Strohmayer & Brown 2002). The disintegration of heavy rapid proton capture process (rp-process) ashes can provide up to half of the observed energy (Schatz et al. 2003a). Because superbursts ignite very close to the outer neutron star crust, they offer the opportunity to probe crust properties such as thermal structure and conductivity (Brown 2004; Cumming et al. 2006) or physics at the interface between the liquid ocean and the solid crust (Horowitz et al. 2007; Medin & Cumming 2011). Keek & Heger

(2011) demonstrated the sensitivity of superburst light curves and recurrence times on the heat flux emerging from the outer crust, through its effect on the ignition depth.

The carbon ignition model explains nicely the energetics and the long burst duration that corresponds to the thermal timescale for cooling such a thick carbon enriched layer. By comparing observed light curves to superburst models, Cumming & Macbeth (2004) and Cumming et al. (2006) obtain ignition column depths of $0.5\text{--}3 \times 10^{12} \text{ g cm}^{-2}$. For typical accretion rates, this is consistent with the estimated recurrence times of the order of a year. Complete superburst light curves from ignition to late time cooling have been modeled by Weinberg & Bildsten (2007). More recently, first multi-zone calculations of superbursts have been carried out (Keek & Heger 2011). The models agree reasonably well with observed burst light curves but only when using larger than observed accretion rates.

There are also a number of problems with the carbon ignition model. Besides insufficient heating leading to too long recurrence times (Keek et al. 2008; Kuulkers et al. 2010), the most obvious open question is the production mechanism for the large amounts of carbon (mass fraction $X_C = 10\text{--}20\%$) needed to ignite the superbursts (Cumming et al. 2006). Understanding the origin of the carbon is important to support the carbon ignition model as an explanation for superbursts in general, and to constrain the carbon fraction when modeling superbursts for comparison with observations. In this work we use updated nuclear reaction rates and explore systematically carbon production in stable, steady state nuclear burning for a much wider range of parameters that covers not only mixed hydrogen and helium accretors, but also

helium accreting UCXBs. In addition we investigate the sensitivity of carbon production to the underlying nuclear physics for the entire parameter space and identify nuclear reaction rates that should be better constrained to reliably predict carbon production for superbursts.

2. CARBON PRODUCTION IN RP-PROCESS BURNING

Most superbursts occur on neutron stars that accrete a mix of hydrogen and helium at a typical rate of $0.1\text{--}0.3 \dot{m}_{\text{Edd}}$ (Falanga et al. 2008), with \dot{m}_{Edd} being the Eddington accretion rate for solar composition $\dot{m}_{\text{Edd}} \approx 10^5 \text{ g cm}^{-2} \text{ s}^{-1}$. In this case carbon has to be produced by thermonuclear burning of hydrogen and helium near the neutron star surface. One option are the regular type I bursts that these systems exhibit. However, state of the art X-ray burst models produce at most a few percent ^{12}C (Schatz et al. 2003b; Woosley et al. 2004; Fisker et al. 2008; José et al. 2010). At the end of the burst the ashes contains a mix of ^{12}C and unburned ^4He . Woosley et al. (2004) showed that $^{12}\text{C}+^4\text{He}$ reactions triggered by heating from subsequent bursts on top of the ashes further reduce X_{C} to negligible values.

Medin & Cumming (2011) recently suggested that in steady-state the preferential crystallization of heavy nuclei at the ocean crust interface (Horowitz et al. 2007) might lead to mixing and an enrichment of light nuclei in the liquid phase. The results imply that material with X_{C} of just a few percent could be enriched to as much as 40% at the depth where superbursts ignite. However, the total amount of carbon needed to explain the energetics of the observed superbursts remains the same. If carbon production is a factor of 10 lower then the time to accumulate the required amount of carbon will increase by a factor of 10, making recurrence times longer than observed.

Some superburst have been observed in X-ray bursting ultra compact X-ray binaries (UCXB), for example in 4U 0614+91 (Kuulkers et al. 2010) and 4U 1820-30 (Strohmayer & Brown 2002). These systems are characterized by very low orbital periods that imply a compact companion star without a hydrogen envelope. Most neutron stars in UCXBs are therefore thought to accrete mainly ^4He . One might expect that helium driven X-ray bursts are a more favorable environment for carbon production due to the low $^{12}\text{C}(\alpha, \gamma)$ reaction rate creating a bottleneck in the helium burning reaction sequence. However, Weinberg et al. (2006) showed that $^{12}\text{C}(\alpha, \text{p})^{15}\text{N}(\text{p}, \gamma)^{16}\text{O}$, enabled by a very low abundance of hydrogen produced by (α, p) reactions, serves as an effective bypass of the $^{12}\text{C}(\alpha, \gamma)$ reaction, resulting in negligible amounts of ^{12}C ($X_{\text{C}} < 10^{-5}$) being produced in helium burning X-ray bursts. ^4He driven X-ray burst can also occur in mixed hydrogen and helium accretors at low accretion rates and high metallicities, when hydrogen burning via the CNO cycle prior to burst ignition consumes all hydrogen. The environment is somewhat different to pure helium accretors as mixing with hydrogen-rich surface layers alters the nucleosynthesis. Woosley et al. (2004) find a carbon production of at most a few percent for such bursts.

We conclude that neither mixed hydrogen and helium bursts, nor pure helium flashes can produce the amounts

of carbon required for superbursts. Kuulkers et al. (2010) explored the possibility that the explosion of a cold, thick helium layer is responsible for a superburst observed in the UCXB 4U 0614+091. While this model can explain the observed features it would require a nuclear energy generation rate of only 0.6 MeV u^{-1} , almost a factor 3 lower than what is expected from helium burning. In addition, the model requires atypically low accretion rates around $0.004 \dot{m}_{\text{Edd}}$ and is therefore only applicable for the special case of 4U 0614+091. Cooper et al. (2009) explored alternative triggers for superbursts, including temperature sensitive electron capture rates and $^{12}\text{C}+^4\text{He}$ reactions. They find that none of these can explain superburst observables, and conclude that deep carbon burning is the only viable model.

It has been suggested that stable burning of hydrogen or helium is the source of carbon powering superbursts (Strohmayer & Brown 2002; Schatz et al. 2003b). While all superbursting systems show regular type I X-ray bursts this does not necessarily mean that all the accreted fuel is burned explosively in bursts. in't Zand et al. (2003) demonstrated that for all seven superbursting systems they investigated the observed ratio of the bolometric persistent X-ray emission, powered by gravitational energy release, and the bolometric summed X-ray emission of all X-ray bursts, powered by nuclear burning, is high, of the order of $\alpha \approx 1000$. Such high α values are typical for the mixed hydrogen and helium accretors with accretion rates around $0.1\text{--}0.3 \dot{m}_{\text{Edd}}$ that host the majority of superbursts. If all accreted fuel were burned in X-ray bursts, one would expect $\alpha \approx 40$ — the ratio of gravitational energy release (about 200 MeV u^{-1}) and nuclear energy release (about 5 MeV u^{-1} for hydrogen burning). Such α values are typical for systems that show regular X-ray bursts only. The high α values in superbursting systems therefore indicate that a large fraction of the accreted hydrogen and helium is burned stably.

For the helium accreting UCXB 4U 1820-30 Cumming (2003) find $\alpha = 150$, not too far from what is expected for helium burning. However, the system is known to spend a significant amount of time in a high accretion rate state where bursts disappear. It is therefore possible, that the carbon powering the superburst observed during the low accretion rate phase has been formed mainly during stable burning in the high accretion rate phase (Strohmayer & Brown 2002).

While observations clearly indicate some stable burning in the accretion rates regime around $0.1\text{--}0.3 \dot{m}_{\text{Edd}}$ relevant for super bursts, theoretical considerations (Fujimoto et al. 1981; Bildsten 1998) and time dependent models of accreting neutron stars (Fisker et al. 2007; Heger et al. 2007) indicate a transition to stable burning at much higher accretion rates, around $1 \dot{m}_{\text{Edd}}$. The origin of this discrepancy is not understood. Schatz et al. (1999) calculated the nucleosynthesis during stable burning of hydrogen and helium in solar proportions using a steady-state burning model that assumes the burning to be stable. Calculations were performed for a range of accretion rates above $1 \dot{m}_{\text{Edd}}$ and X_{C} was found to be at most 6%. Only the $^{15}\text{O}(\alpha, \gamma)$ reaction rate was varied to explore nuclear physics uncertainties. The parameter range was extended to lower accretion rates in Schatz et al. (2003b), who found $X_{\text{C}} > 10\%$ for accretion rates

below $0.3 \dot{m}_{\text{Edd}}$. This confirmed that steady-state burning is a viable mechanism for producing larger amounts of carbon on accreting neutron stars at the typical accretion rates of superburst systems.

3. CALCULATIONS OF STABLE RP-PROCESS BURNING

We use the same model described in Schatz et al. (1999) to calculate the nucleosynthesis in steady-state nuclear burning on an accreting neutron star. The model determines the temperature profile by integrating the radiation flux generated by nuclear reactions from the surface down to a depth where all fuel is burned. Nuclear reactions are followed with a detailed nuclear reaction network including 686 nuclei from hydrogen to tellurium using the reactions in JINA reaclib version 1.0 rates (Cyburt et al. 2010).

The surface gravity is fixed to a typical value of $g = 2.42 \times 10^{14} \text{ g cm}^{-2}$ for a canonical neutron star with a mass of $1.4 M_{\odot}$ and a 10 km radius, taking into account relativistic corrections. This leaves three free parameters, the heat flux entering the surface layers from the crust F_b , the accretion rate \dot{m} , and the composition of the accreted material, in particular the helium mass fraction X_{He} .

F_b is the portion of the heat generated by electron captures and pycnonuclear fusion reactions deeper in the crust that emerges at the surface of the crust. F_b depends on the heating and cooling reactions in the crust and the crust's thermal conductivity. We explore a typical range of $F_b = 1, 50, 100, 500$, and 1000 keV u^{-1} (Brown 2000) similar to the range used in studies of superbursts (Keek & Heger 2011).

The electron scattering, free-free absorption, and conduction opacity calculations used in this study are detailed in Schatz et al. (1999). However, Schatz et al. (1999) assumed that the total Rosseland mean radiative opacity was given by the sum of the electron scattering and free-free Rosseland mean opacities $\kappa = \kappa_{\text{es}} + \kappa_{\text{ff}}$. In fact, as discussed by Potekhin & Yakovlev (2001), the Rosseland means do not add in this way, as the Rosseland mean of the opacity sum is not the same as the sum of the Rosseland means. A direct sum of the Rosseland means underestimates the opacity by about 30 % when the electron scattering and free-free contributions are comparable. To correct for this, we adopt the “non-additivity” factor of Potekhin & Yakovlev (2001) (see their eq. [20]). The new opacity is slightly higher (Fig. 1), however, the results are essentially the same as the ones obtained with the opacities from Schatz et al. (1999).

We express \dot{m} in multiples of $\dot{m}_{\text{Edd}} = 87900 \text{ g cm}^{-2} \text{ s}^{-1}$, which is the local Newtonian Eddington accretion rate for solar composition, and provides a convenient scale. We vary \dot{m} from 0.1 to $40 \dot{m}_{\text{Edd}}$. $\dot{m} = 0.1\text{--}0.3 \dot{m}_{\text{Edd}}$ are typical values for superbursting systems. However, these accretion rates are derived from the inferred global accretion rate assuming the local accretion rate is the same across the neutron star surface. This might not always be the case. The fact that X-ray burst models only show stable burning at accretion rates significantly above $\dot{m} = 0.1\text{--}0.3 \dot{m}_{\text{Edd}}$ (Bildsten 1998; Fisker et al. 2003) might be a hint that local accretion rates are higher than expected. To cover this possibility we therefore

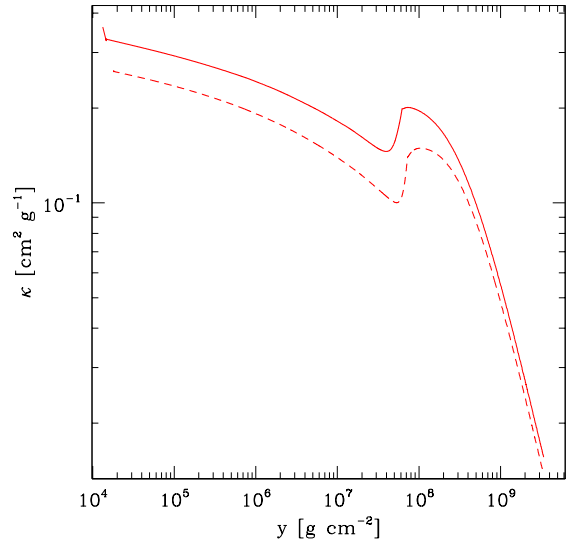


FIG. 1.— The opacity as a function of column depth at $X_{\text{He}} = 0.5$ and $\dot{m} = 0.3 \dot{m}_{\text{Edd}}$ using the opacities from Schatz et al. (1999) with (solid) and without (dashed) the non-additivity factor from Potekhin & Yakovlev (2001).

explore also the consequences of higher local accretion rates.

Accretion from normal main sequence stars likely leads to an accreted composition close to solar. The composition accreted from a compact helium star in a UCXB is expected to be dominated by ^4He . Depending on the evolutionary path that formed the system, a hydrogen mass fraction between close to zero and 40 % (Cumming 2003) is possible. To explore the entire parameter space we use solar metallicity throughout (a test run with reduced metallicity did not show any significant differences) and vary the hydrogen mass fraction from solar to zero. This results in a X_{He} range of 0.28–0.98.

To explore the sensitivity of carbon production to nuclear reaction rates, we vary individual reaction rates that lie along the reaction path one by one by factors of 10 up and down. The rate variations are performed for a range of models on a reduced grid of input parameters. We kept $F_b = 1 \text{ keV u}^{-1}$ as X_C was found to not depend significantly on F_b . For X_{He} we chose a low and a high value, 0.3, and 0.9. We then used as models for the rate variations $\dot{m} = 0.1, 0.5, 1, 2, 5 \dot{m}_{\text{Edd}}$ and $\dot{m} = 0.1, 0.5, 1, 2, 5, 10, 20, 30 \dot{m}_{\text{Edd}}$ for low and high X_{He} , respectively. For low X_{He} a more limited \dot{m} range is used as carbon production is negligible for $\dot{m} > 5 \dot{m}_{\text{Edd}}$.

4. CARBON SYNTHESIS IN STEADY-STATE RP-PROCESS BURNING

Schatz et al. (1999) already described the reaction sequences during steady-state burning of a solar hydrogen and helium mixture. Helium burns mainly by the 3α reaction and the αp process (Wallace & Woosley 1981), a sequence of (α, p) and (p, γ) reactions. The endpoint of the αp process depends very sensitively on peak temperature and therefore on accretion rate. Higher accretion rates result in a higher nuclear energy production rate generating more flux and therefore require a steeper temperature profile resulting in a higher burning temperature (Fig. 2). Hydrogen burns at low accretion rates via the CNO cycles and at higher accretion rates via

the rapid proton capture process (rp-process) (Wallace & Woosley 1981), a sequence of rapid proton captures and slower β^+ decays.

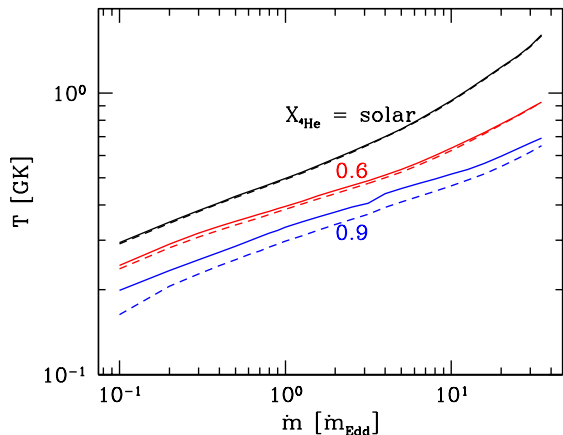


FIG. 2.— Temperature as a function of accretion rate from the time H is reduced to 90 % of its initial abundance to the time carbon is built up to 90 % of its final abundance for $X_{\text{He}} = \text{solar}$ (black), 0.6 (red), 0.9 (blue). Solid is the temperature at 90 % carbon and dashed is the temperature at 90 % hydrogen.

Carbon is produced directly by the 3α reaction but is destroyed rapidly by the $^{12}\text{C}(p,\gamma)^{13}\text{N}$ reaction as long as any hydrogen is present. However, the rate of the 3α reaction is proportional to X_{He}^3 and therefore decreases rapidly as ^4He is consumed. Therefore ^4He burns at late times much slower than hydrogen. The main source of carbon in the ashes is then 3α burning that occurs after the rp-process has consumed all the hydrogen.

The amount of carbon synthesized is determined by several factors. One important factor is the amount of helium present at the time of hydrogen exhaustion, which depends mainly on the speed of the rp-process versus the 3α process. A slower rp-process leads to more helium burning before hydrogen is exhausted and therefore less remaining carbon. The rp-process waiting points therefore play a critical role. The second factor is the rate of carbon destruction through $^{12}\text{C}(\alpha,\gamma)^{16}\text{O}$ once hydrogen is consumed, which depends on the temperature and density after hydrogen exhaustion (Schatz et al. 1999). In addition, any helium producing hydrogen burning reaction sequences such as the CNO or the SnSbTe cycles (Schatz et al. 2001) will favor carbon synthesis.

4.1. Trends in Carbon Production with \dot{m} , X_{He} , and F_b

Fig. 3 shows the ^{12}C mass fraction produced in steady-state burning at $F_b = 1.0 \text{ keV u}^{-1}$. There are two overall trends. First, X_C increases with the initial X_{He} as higher X_{He} results in more helium being present at the point of hydrogen exhaustion. There are a number of reasons for this behavior. A higher initial X_{He} simply leads to higher X_{He} throughout and therefore to more helium for carbon production. Helium burning also generates less energy than hydrogen burning. Therefore, a higher initial X_{He} leads to lower burning temperatures, and less helium destruction via $^{12}\text{C}(\alpha,\gamma)$. Lower temperatures also lead to a shorter αp -process, a lower proton to seed ratio, and therefore a shorter rp-process, which accelerates hydrogen burning favoring carbon production.

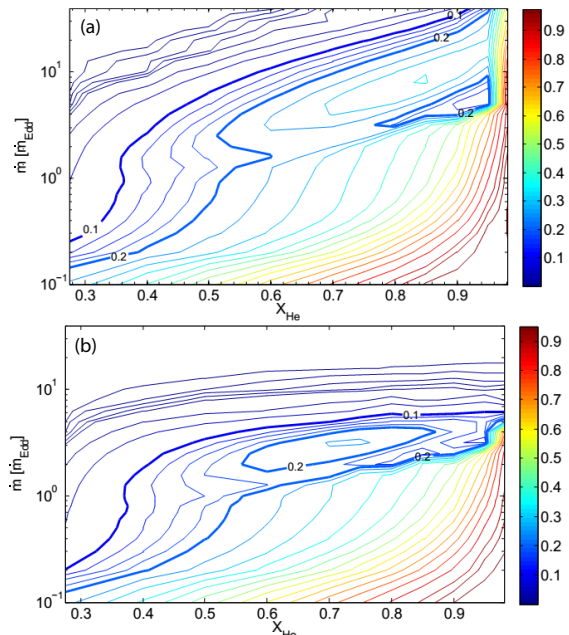


FIG. 3.— Final ^{12}C mass fraction as function of accretion rate and initial helium mass fraction at $F_b = 1 \text{ keV u}^{-1}$ (a) and $F_b = 1 \text{ MeV u}^{-1}$ (b). Contours are in steps of 0.0025 from 0.001 to 0.01, in steps of 0.025 from 0.01 to 0.2, in steps of 0.05 from 0.2 to 0.9. Additional contours are drawn at 0.925, 0.95, 0.9625, 0.975 and 1. Mass fractions of 10 % and 20 % are bolded and labeled.

The second general trend in Fig. 3 is an increasing X_C with decreasing \dot{m} . One reason is that carbon production is favored at lower temperatures (see arguments above). In addition, at low \dot{m} hydrogen burning via the rp-process sets in at much later times, resulting in more hydrogen burned via the CNO cycle prior to ignition of the rp-process, further increasing X_{He} .

Carbon production depends only modestly on F_b (Fig. 3). The biggest difference occurs for $\dot{m} > 10 \dot{m}_{\text{Edd}}$ where for $F_b = 1 \text{ MeV u}^{-1}$ carbon production rapidly goes to zero regardless of composition, while for $F_b = 1 \text{ keV u}^{-1}$ for $X_{\text{He}} > 0.6$ still more than 10% carbon can be made. The reason is that for a significant F_b the temperature will continue to raise beyond the depth of the main nuclear energy generation, leading to more efficient burning of the remaining carbon and helium.

4.2. An Island of Lower Carbon Production

There is a narrow range of accretion rates — around $1 \dot{m}_{\text{Edd}}$ for near solar X_{He} increasing to around $8\text{--}10 \dot{m}_{\text{Edd}}$ for helium-rich environments — where less carbon is produced than is expected from the general trends. For low X_{He} this is just a small dip, but for larger X_{He} the reduction in carbon production is substantial. This gives rise to an island of low carbon mass fraction in the contours of Fig. 3.

The reason for this behavior is the interplay between the $^{14}\text{O}(\alpha,p)^{17}\text{F}$ reaction and the $^{12}\text{C}(p,\gamma)^{13}\text{N}(\alpha,p)^{16}\text{O}$ carbon destruction sequence once most of the hydrogen is consumed. The destruction of carbon via $^{12}\text{C}(p,\gamma)^{13}\text{N}(\alpha,p)^{16}\text{O}$ requires only a very small abundance of hydrogen (Weinberg et al. 2006), since hydrogen merely is needed as a catalyst. For some accretion rates the $^{14}\text{O}(\alpha,p)^{17}\text{F}$ reaction can maintain such a small proton abundance during the helium burning phase, re-

ducing the amount of carbon that can be produced. This can be seen in Fig. 4. After hydrogen burning, as ^{14}O is depleted, the hydrogen abundance starts increasing again reaching abundances around 10^{-6} . During this time, the carbon abundance is significantly reduced. The hydrogen abundance level that can be maintained by the $^{14}\text{O}(\alpha, p)^{17}\text{F}$ reaction also depends on the rate of the $^{17}\text{F}(\text{p}, \gamma)$ reaction. Once ^{14}O is depleted, $^{17}\text{F}(\text{p}, \gamma)$ destroys the remaining hydrogen and carbon production increases again, however, the final carbon abundance is significantly reduced.

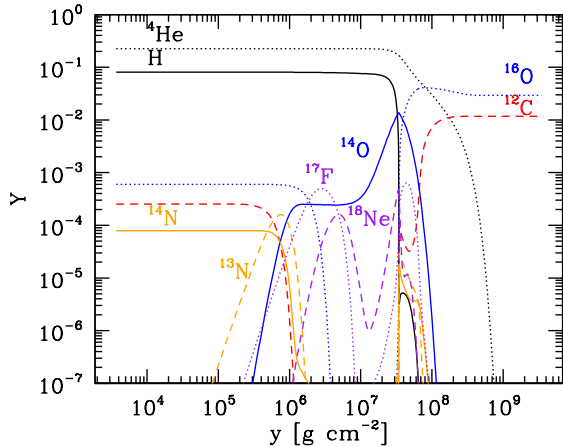


FIG. 4.— Abundances of H, He, ^{12}C , ^{13}N , ^{14}N , ^{14}O , ^{16}O , ^{17}F , and ^{18}Ne as functions of column depth, represented by black(s), black(d), red(s), orange(s), orange(d), blue(s), blue(do), indigo(do), and indigo(d) lines, respectively, with “s”, “d”, and “do” indicating solid, dashed, and dotted respectively. Conditions correspond to the island of low carbon production, $F_b = 1 \text{ keV u}^{-1}$ and $\dot{m} = 5 \dot{m}_{\text{Edd}}$.

The effect can only occur for a narrow range of accretion rates where at the time of hydrogen exhaustion a substantial amount of ^{14}O has build up and starts burning via $^{14}\text{O}(\alpha, p)$. For lower accretion rates and lower temperatures, $^{14}\text{O}(\alpha, p)$ will not occur during helium burning, or, ^{14}O is not produced at all. For higher accretion rates and higher temperatures $^{14}\text{O}(\alpha, p)$ breakout occurs prior to hydrogen exhaustion destroying all ^{14}O . In principle (α, p) reactions on heavier nuclei serve then as sources of protons. However, the proton abundance level that is reached never exceeds 10^{-8} , which is not sufficient to trigger the $^{12}\text{C}(\text{p}, \gamma)^{13}\text{N}(\alpha, p)^{16}\text{O}$ carbon destruction sequence.

5. REACTION RATE SENSITIVITY

To better understand the dependence of the synthesis of carbon on nuclear reactions, and to identify bottleneck reactions we varied all reaction rates with significant reaction flow by a factor of 10 up and down for a set of accretion rates and initial compositions of $X_{\text{He}} = 0.9$ (helium-rich environment) and $X_{\text{He}} = 0.275$ (hydrogen-rich environment). All important reaction rates that change the final ^{12}C mass fraction by more than 5% when varied by a factor of 10 are summarized in Table 1, along with the maximum change in carbon mass fraction.

At low accretion rates nuclear processing is largely dominated by the hot CNO cycle with the β -decays of ^{14}O and ^{15}O being the only reactions controlling carbon

TABLE 1
REACTIONS IMPACTING CARBON PRODUCTION BY MORE THAN 5% WHEN VARIED BY A FACTOR OF 10 FOR CONDITIONS WHERE MORE THAN $X_{\text{C}} = 0.01$ IS PRODUCED.

Reaction	$\times 10^a$	$/10^b$	Experimentally uncertain rate
$^{12}\text{C}(\text{p}, \gamma)^{13}\text{N}$	0.04	2.58	
$^{13}\text{N}(\text{p}, \gamma)^{14}\text{O}$	0.77	1.12	
$^{13}\text{N}(\alpha, p)^{16}\text{O}$	1.12	0.75	Yes
$^{14}\text{O}(\beta^+)^{14}\text{N}$	3.83	0.19	
$^{14}\text{O}(\alpha, p)^{17}\text{F}$	2.70	2.79	Yes
$^{15}\text{O}(\beta^+)^{15}\text{N}$	2.00	0.30	
$^{18}\text{F}(\beta^+)^{18}\text{O}$	0.94	1.12	
$^{18}\text{Ne}(\beta^+)^{18}\text{F}$	1.40	0.17	
$^{19}\text{F}(\text{p}, \alpha)^{16}\text{O}$	≈ 1	0.88	
$^{19}\text{Ne}(\beta^+)^{19}\text{F}$	0.64	0.79	
$^{22}\text{Na}(\text{p}, \gamma)^{23}\text{Mg}$	1.54	0.77	
$^{22}\text{Na}(\alpha, p)^{25}\text{Mg}$	1.09	1.23	Yes
$^{43}\text{Ti}(\text{p}, \gamma)^{44}\text{V}$	≈ 1	1.14	Yes
$^{52}\text{Fe}(\text{p}, \gamma)^{53}\text{Co}$	≈ 1	0.94	Yes
$^{57}\text{Ni}(\text{p}, \gamma)^{58}\text{Cu}$	≈ 1	0.92	Yes
$^{61}\text{Ga}(\beta^+)^{61}\text{Zn}$	1.06	≈ 1	
$^{64}\text{Ge}(\beta^+)^{64}\text{Ga}$	1.09	0.84	
$^{66}\text{Ge}(\text{p}, \gamma)^{67}\text{As}$	≈ 1	0.95	Yes
$^{68}\text{Se}(\beta^+)^{68}\text{As}$	≈ 1	0.94	

^a Factor of change in X_{C} when increasing rate by a factor of 10

^b Factor of change in X_{C} when decreasing rate by a factor of 10

production (Fig. 5). At somewhat higher accretion rates (starting at 2 and $0.5 \dot{m}_{\text{Edd}}$ in helium and hydrogen-rich environments, respectively) $^{12}\text{C}(\text{p}, \gamma)$ becomes one of the most important reactions as the primary destruction mechanism for carbon.

In helium-rich material the $^{14}\text{O}(\alpha, p)$ triggered carbon depletion effect discussed above occurs at accretion rates in the $5\text{--}20 \dot{m}_{\text{Edd}}$ range. Under those conditions the proton production reaction rate $^{14}\text{O}(\alpha, p)^{17}\text{F}$ and the rates of the carbon destruction sequence $^{12}\text{C}(\text{p}, \gamma)$ and $^{13}\text{N}(\alpha, p)$ become important. In addition the ^{19}Ne β -decay and the $^{19}\text{F}(\text{p}, \alpha)$ reaction rates are important, as these reactions form an additional pathway to produce helium thereby increasing final carbon production. However, the impact of the reaction rates in such cycles is not obvious as the impact from the increased helium production can be offset by the slower hydrogen burning in the cycle compared to the more rapid hydrogen burning reactions sequences of the rp-process. For example, a decreased $^{19}\text{F}(\text{p}, \alpha)$ rate decreases carbon production, while both, and increased and a decreased ^{19}Ne β -decay rate decrease carbon production.

In helium-rich environments at very high accretion rates of $30 \dot{m}_{\text{Edd}}$ the NeNa cycle (Marion & Fowler 1957) becomes important (Fig. 5), resulting in sensitivity of carbon production to the rates of the $^{22}\text{Na}(\text{p}, \gamma)$ and $^{22}\text{Na}(\alpha, p)$ breakout reaction rates.

In hydrogen-rich environments more complex reaction sequences develop (Fig. 5). Already between $0.1\text{--}0.5 \dot{m}_{\text{Edd}}$ breakout from the CNO cycles occurs. At $0.5 \dot{m}_{\text{Edd}}$ $^{14}\text{O}(\alpha, p)$ becomes important causing the additional carbon depletion effect described above. The $^{43}\text{Ti}(\text{p}, \gamma)$ reaction rate becomes also important determining breakout from the CaSc (van Wormer et al. 1994) cycle. This cycle slows down hydrogen burning and increases helium production. In addition rp-process bot-

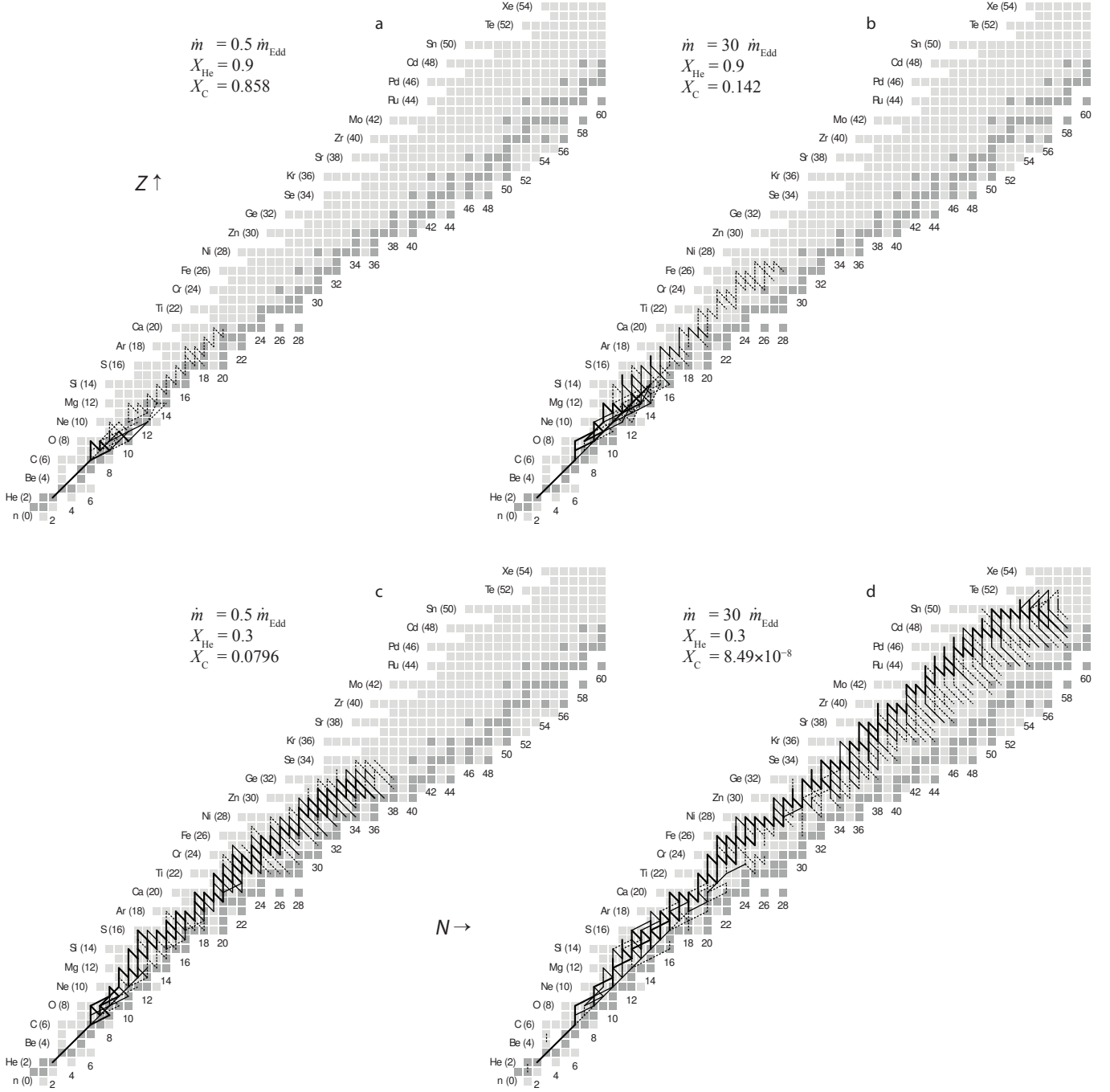


FIG. 5.— Time-integrated reaction flows for (a) $X_{\text{He}} = 0.9$, $\dot{m} = 0.5 \dot{m}_{\text{Edd}}$; (b) $X_{\text{He}} = 0.9$, $\dot{m} = 30 \dot{m}_{\text{Edd}}$; (c) $X_{\text{He}} = 0.3$, $\dot{m} = 0.5 \dot{m}_{\text{Edd}}$; and (d) $X_{\text{He}} = 0.3$, $\dot{m} = 30 \dot{m}_{\text{Edd}}$. The final ^{12}C mass fractions for these runs are $X_{\text{C}} = 0.858, 0.142, 0.0796,$ and 8.49×10^{-8} , respectively.

tleneck reactions such as $^{57}\text{Ni}(p, \gamma)$ start controlling carbon production. For such rp-process bottle-necks, an increased rate leads to more rapid hydrogen burning, earlier hydrogen consumption, higher helium abundance at the time of hydrogen depletion, and therefore increased carbon production.

At higher accretion rates of $2 \dot{m}_{\text{Edd}}$ the important rp-process bottlenecks are the β^+ decays of ^{61}Ga , ^{64}Ge , and ^{68}Se . The sensitivity to the ^{18}Ne β^+ decay rate indicates the importance of the extended CNO cycle. At still higher accretion rates carbon production is of the order of a percent or less and therefore negligible.

The (α, p) and (β^+) reactions on ^{14}O at high He mass fractions and around $\dot{m} = 5$ and $10 \dot{m}_{\text{Edd}}$ have the largest impact on carbon production. The $^{14}\text{O}(\alpha, p)^{17}\text{F}$ reaction has the largest impact on carbon production because changes in its rate shift the conditions where the released protons can lead to additional carbon destruction. As Fig. 6 and 7 show, a higher rate shifts the narrow parameter space for additional carbon destruction to lower \dot{m} as the rate becomes already effective at lower temperatures. At the same time the strength of the effect is reduced as the higher rate results in a reduced buildup of ^{14}O . For helium-rich environments

($X_{\text{He}} > 0.5$) with some small admixture of hydrogen a high $^{14}\text{O}(\alpha, p)^{17}\text{F}$ therefore allows for the production of large amounts of carbon $X_{\text{C}} > 20\%$ even at very high accretion rates ($3\text{--}20 \dot{m}_{\text{Edd}}$ depending on X_{He}) beyond the narrow $^{14}\text{O}(\alpha, p)^{17}\text{F}$ carbon destruction region. For a low $^{14}\text{O}(\alpha, p)^{17}\text{F}$ reaction rate carbon production is much reduced for high accretion rates.

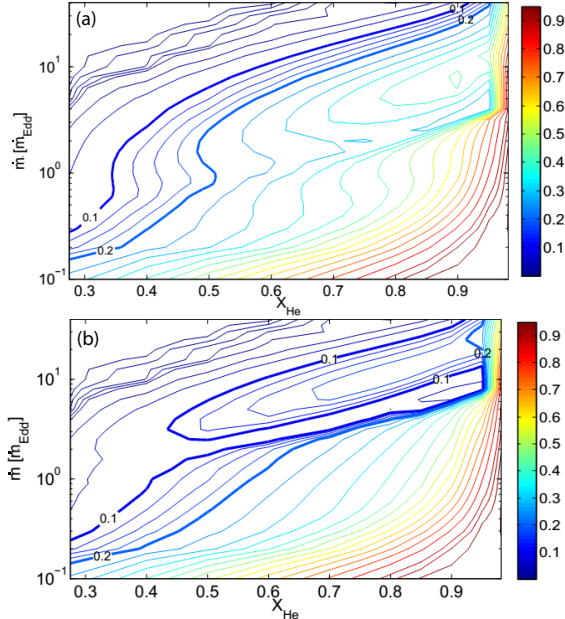


FIG. 6.— Final ^{12}C mass fraction as function of accretion rate and initial helium mass fraction at $F_{\text{b}} = 1 \text{ keV u}^{-1}$ with the $^{14}\text{O}(\alpha, p)^{17}\text{F}$ reaction rate increased (a) and decreased (b) by a factor of 10. See Fig. 3 for contour details.

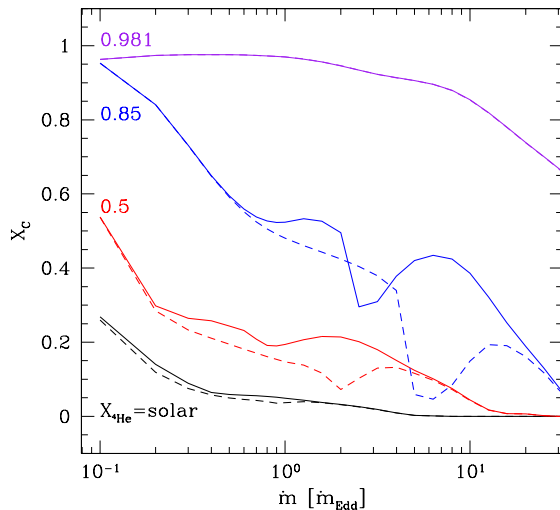


FIG. 7.— Carbon mass fraction X_{C} as a function of accretion rate \dot{m} for several initial X_{He} and for the $^{14}\text{O}(\alpha, p)^{17}\text{F}$ reaction rate increased by a factor of 10 (solid lines) and decreased by a factor of 10 (dashed lines). Black, red, blue, and purple lines represent, in order, $X_{\text{He}} = \text{solar}$, 0.5, 0.85, and 0.98.

Except for the narrow region of additional carbon destruction, a large $^{14}\text{O}(\alpha, p)^{17}\text{F}$ reaction rate therefore increases carbon production in most areas of the parameter space. This is also true for lower accretion rates below

the carbon destruction region, even for hydrogen-rich environments. In this regime a higher $^{14}\text{O}(\alpha, p)^{17}\text{F}$ rate will reduce the buildup of ^{14}O , and therefore the amount of protons released, once hydrogen is consumed. While at the lower temperatures in this accretion rate regime the $^{12}\text{C}(p, \gamma)^{13}\text{N}(\alpha, p)^{16}\text{O}$ chain cannot be triggered, proton production will still lead to some carbon destruction.

6. CONCLUSIONS

We have explored carbon production in steady-state hydrogen and helium burning. We find that large amounts of carbon $X_{\text{C}} > 10\text{--}20\%$ sufficient for igniting superbursts are produced for a wide range of parameters. While carbon production increases with X_{He} in the accreted material, we find that even for solar composition $X_{\text{C}} > 10\%$ for $\dot{m} < 0.28 \dot{m}_{\text{Edd}}$. Therefore, steady-state burning is expected to produce enough carbon to power superbursts for typical observationally inferred accretion rates, assuming the accretion rate at the depth of nuclear burning is the same across the neutron star surface.

The problem remains that current models do not predict steady-state burning at such low accretion rates even though it is observed. One possible solution is rotationally induced mixing that transports fuel to greater depths more efficiently (Keek et al. 2009). Another possibility is that anisotropies in the accretion rate persist to the depth of nuclear burning leading to higher local accretion rates in certain regions (Bildsten 1998). However, our results indicate that in such cases, the accreted material must be depleted in hydrogen to produce large amounts of carbon. For example, at a local accretion rate of $1 \dot{m}_{\text{Edd}}$, roughly where models predict the transition to stable burning (Bildsten 1998), depending on the value of the $^{14}\text{O}(\alpha, p)$ reaction rate, $X_{\text{He}} > 0.36\text{--}0.4$ is required to produce $X_{\text{C}} > 0.1$. Higher local accretion rates will require even higher X_{He} .

We also find that carbon production is reduced for certain accretion rates due to proton production via the $^{14}\text{O}(\alpha, p)$ reaction at late times, once hydrogen has been consumed. The effect on carbon production is particularly pronounced if the $^{14}\text{O}(\alpha, p)$ reaction rate is a factor of 10 lower than currently estimated. In this case, the only way to produce $X_{\text{C}} \approx 20\%$ at accretion rates beyond $10 \dot{m}_{\text{Edd}}$ is for a pure helium composition.

We identified the critical nuclear physics that controls carbon production in steady-state burning. A quantitative determination of the nuclear physics uncertainty in X_{C} would require a Monte Carlo study where all reaction rates are varied randomly for all conditions. This is beyond the scope of this study. Nevertheless we can use the results of our sensitivity study to identify sources of uncertainty that need to be addressed for a reliable prediction of carbon production in this scenario.

Among the reactions listed in Table 1 the β^+ decay rates are not expected to be major sources of uncertainty. All the rates listed are well known experimentally. Terrestrial electron capture contributions are expected to be small, and the nuclei do not have low lying excited states that could be thermally populated in a significant way. Therefore modifications to these decay rates due to the high densities and temperatures in the astrophysical environment are expected to be small.

The reaction rates for proton capture on ^{12}C , ^{13}N , and

^{22}Na as well as $^{19}\text{F}(\text{p},\alpha)$ are relatively well experimentally studied with uncertainties of the order of 25 % or less (Angulo et al. 1999; Iliadis et al. 2010; Xu et al. 2012; La Cognata et al. 2011). Considering the impact that a factor of 10 variation of these rates have on carbon production we conclude that their uncertainties affect X_{C} by less than 5 % and are therefore negligible.

For the remaining reaction rates experimental information is sparse or non existent and assuming an uncertainty of the order of a factor of 10 is not unreasonable. These reaction rates introduce uncertainties of the order of 5–10 % or more in X_{C} and are marked in Table 1. Only the uncertainty of the $^{14}\text{O}(\alpha,\text{p})$ reaction rate affects X_{C} by more than 50 %. It should be noted that for most of these reactions estimates of the uncertainty are highly uncertain themselves, and that larger deviations from the true rate are not unlikely. A better experimental determination of these reaction rates would

significantly improve the reliability of predictions of carbon production in steady-state burning of hydrogen and helium.

We thank L. Bildsten, L. Keek, and Z. Meisel for useful discussions, and F.-K. Thielemann for providing the reaction network solver. A. Cumming is supported by an NSERC Discovery Grant and is an Associate Member of the CIFAR Cosmology and Gravity program. E. F. Brown is supported NSF AST grant 11-09176. E. F. Brown and A. Cumming are grateful to the International Space Science Institute (ISSI) in Bern for the support of an International Team on Type I X-ray Bursts. This work was supported by NSF grants PHY 08-22648 (Joint Institute for Nuclear Astrophysics) and NSF PHY 11-0251.

REFERENCES

- Angulo, C., Arnould, M., Rayet, M., et al. 1999, *Nuclear Physics A*, 656, 3
- Bildsten, L. 1998, in *NATO ASIC Proc. 515: The Many Faces of Neutron Stars.*, ed. R. Buccheri, J. van Paradijs, & A. Alpar, 419
- Brown, E. F. 2000, *ApJ*, 531, 988
- Brown, E. F. 2004, *ApJ*, 614, L57
- Cooper, R. L., Steiner, A. W., & Brown, E. F. 2009, *ApJ*, 702, 660
- Cornelisse, R., Heise, J., Kuulkers, E., Verbunt, F., & in't Zand, J. J. M. 2000, *A&A*, 357, L21
- Cornelisse, R., Kuulkers, E., in't Zand, J. J. M., Verbunt, F., & Heise, J. 2002, *A&A*, 382, 174
- Cumming, A. 2003, *ApJ*, 595, 1077
- Cumming, A., & Bildsten, L. 2001, *ApJ*, 559, L127
- Cumming, A., & Macbeth, J. 2004, *ApJ*, 603, L37
- Cumming, A., Macbeth, J., in't Zand, J. J. M., & Page, D. 2006, *ApJ*, 646, 429
- Cyburt, R. H., Amthor, A. M., Ferguson, R., et al. 2010, *ApJS*, 189, 240
- Falanga, M., Chenevez, J., Cumming, A., et al. 2008, *Astronomy and Astrophysics*, 484, 43
- Fisker, J. L., Hix, W. R., Liebendörfer, M., & Thielemann, F.-K. 2003, *Nuclear Physics A*, 718, 614
- Fisker, J. L., Schatz, H., & Thielemann, F.-K. 2008, *ApJS*, 174, 261
- Fisker, J. L., Tan, W., Görres, J., Wiescher, M., & Cooper, R. L. 2007, *ApJ*, 665, 637
- Fujimoto, M. Y., Hanawa, T., & Miyaji, S. 1981, *ApJ*, 247, 267
- Galloway, D., in't Zand, J., Chenevez, J., Keek, L., & Brandt, S. 2010, in *COSPAR Meeting, Vol. 38, 38th COSPAR Scientific Assembly*, 2445
- Heger, A., Cumming, A., & Woosley, S. E. 2007, *ApJ*, 665, 1311
- Horowitz, C. J., Berry, D. K., & Brown, E. F. 2007, *Phys. Rev. E*, 75, 066101
- Iliadis, C., Longland, R., Champagne, A. E., Coc, A., & Fitzgerald, R. 2010, *Nuclear Physics A*, 841, 31
- in't Zand, J. J. M., Kuulkers, E., Verbunt, F., Heise, J., & Cornelisse, R. 2003, *A&A*, 411, L487
- José, J., Moreno, F., Parikh, A., & Iliadis, C. 2010, *ApJS*, 189, 204
- Joss, P. C. 1977, *Nature*, 270, 310
- Keek, L., & Heger, A. 2011, *ApJ*, 743, 189
- Keek, L., Heger, A., & in't Zand, J. J. M. 2012, *ApJ*, 752, 150
- Keek, L., & in't Zand, J. J. M. 2008, in *Proceedings of the 7th INTEGRAL Workshop*
- Keek, L., in't Zand, J. J. M., & Cumming, A. 2006, *A&A*, 455, 1031
- Keek, L., in't Zand, J. J. M., Kuulkers, E., et al. 2008, *A&A*, 479, 177
- Keek, L., Langer, N., & in't Zand, J. J. M. 2009, *A&A*, 502, 871
- Kuulkers, E., in't Zand, J. J. M., van Kerkwijk, M. H., et al. 2002, *A&A*, 382, 503
- Kuulkers, E., in't Zand, J. J. M., Atteia, J.-L., et al. 2010, *A&A*, 514, A65
- La Cognata, M., Mukhamedzhanov, A. M., Spitaleri, C., et al. 2011, *ApJ*, 739, L54
- Lewin, W. H. G., van Paradijs, J., & Taam, R. E. 1993, *Space Sci. Rev.*, 62, 223
- Lewin, W. H. G., van Paradijs, J., & van den Heuvel, E. P. J. 1997,
- Maraschi, L., & Cavaliere, A. 1977, in *X-ray Binaries and Compact Objects*, ed. K. A. van der Hucht, 127–128
- Marion, J. B., & Fowler, W. A. 1957, *ApJ*, 125, 221
- Medin, Z., & Cumming, A. 2011, *ApJ*, 730, 97
- Parikh, A., José, J., Sala, G., & Iliadis, C. 2013, *Progress in Particle and Nuclear Physics*, 69, 225
- Potekhin, A. Y., & Yakovlev, D. G. 2001, *A&A*, 374, 213
- Schatz, H., Bildsten, L., & Cumming, A. 2003a, *ApJ*, 583, L87
- Schatz, H., Bildsten, L., Cumming, A., & Ouellette, M. 2003b, *Nuclear Physics A*, 718, 247
- Schatz, H., Bildsten, L., Cumming, A., & Wiescher, M. 1999, *Astrophys. J.*, 524, 1014
- Schatz, H., & Rehm, K. E. 2006, *Nuclear Physics A*, 777, 601
- Schatz, H., Aprahamian, A., Barnard, V., et al. 2001, *Phys. Rev. Lett.*, 86, 3471
- Strohmayer, T. E., & Brown, E. F. 2002, *ApJ*, 566, 1045
- van Wormer, L., Goerres, J., Iliadis, C., Wiescher, M., & Thielemann, F.-K. 1994, *ApJ*, 432, 326
- Wallace, R. K., & Woosley, S. E. 1981, *ApJS*, 45, 389
- Weinberg, N. N., & Bildsten, L. 2007, *ApJ*, 670, 1291
- Weinberg, N. N., Bildsten, L., & Schatz, H. 2006, *ApJ*, 639, 1018
- Woosley, S., & Taam, R. 1976, *Nature*, 263, 101
- Woosley, S., Heger, A., Cumming, A., et al. 2004, *ApJS*, 151, 75
- Xu, Y., Goriely, S., Jorissen, A., Chen, G., & Arnould, M. 2012, *ArXiv e-prints*, arXiv:1212.0628